Increased abundance of Cbl E3 ligases alters PDGFR signaling in recessive dystrophic epidermolysis bullosa

Esther Martínez-Martínez [a], Regine Tölle [a], Julia Donauer [b], Christine Gretzmeier [b], Leena Bruckner-Tuderman [b] and Jörn Dengjel [a]

a - *Department of Biology,* University of Fribourg, Chemin du Musée 10, Fribourg 1700, Switzerland
b - *Department of Dermatology,* Faculty of Medicine, Medical Center-University of Freiburg, Germany

Corresponding author. *joern.dengjel@unifr.ch*.
https://doi.org/10.1016/j.matbio.2021.10.004

Abstract

In recessive dystrophic epidermolysis bullosa (RDEB), loss of collagen VII, the main component of anchoring fibrils critical for epidermal-dermal cohesion, affects several intracellular signaling pathways and leads to impaired wound healing and fibrosis. In skin fibroblasts, wound healing is also affected by platelet-derived growth factor receptor (PDGFR) signaling. To study a potential effect of loss of collagen VII on PDGFR signaling we performed unbiased disease phosphoproteomics. Whereas RDEB fibroblasts exhibited an overall weaker response to PDGF, Cbl E3 ubiquitin ligases, negative regulators of growth factor signaling, were stronger phosphorylated. This increase in phosphorylation was linked to higher Cbl mRNA and protein levels due to increased TGFβ signaling in RDEB. In turn, increased Cbl levels led to increased PDGFR ubiquitination, internalization, and degradation negatively affecting MAPK and AKT downstream signaling pathways. Thus, our results indicate that elevated TGFβ signaling leads to an attenuated response to growth factors, which contributes to impaired dermal wound healing in RDEB.

Introduction

Epidermolysis bullosa (EB) comprises a group of rare inherited skin disorders characterized by mechanically induced blistering and erosions within the skin and mucosal membranes [1]. Among this group, dystrophic epidermolysis bullosa (DEB) is a monogenetic disorder associated with pathogenic variants in the gene encoding collagen VII (COL7A1) [2−4], the main component of anchoring fibrils, which are essential for epidermal-dermal cohesion [5]. The most severe form of the disease is recessive DEB (RDEB). Affected individuals suffer from diminished epidermal-dermal adhesion, skin blistering and subsequent scarring. The continuous damage to the epidermal barrier leads to chronic inflammation and skin infections, which compromise the healing process [6], the result being chronic wounds, progressive scar formation and generalized soft tissue fibrosis [7]. In turn, the inflammatory and fibrotic skin environment favors the development of further disease complications, including squamous cell carcinomas at young ages [8−10]. Despite diverse therapeutic procedures have been tested, such as partly restoring collagen VII (C7) levels, a cure for the disease does not exist and a high unmet medical need persists [11−14]. Promoting proper healing of skin wounds could be fundamental for improved quality of life and prolonged life expectancy of individuals with RDEB. However, to develop effective regenerative therapies, a deeper understanding of the molecular and cellular mechanisms altered in RDEB is absolutely needed.

During the healing process, one of the first growth factors deposited at the wound site by degranulating platelets is platelet-derived growth factor (PDGF), a major mitogen and stimulator of fibroblasts promoting dermal wound healing [15]. The PDGF family of growth factors consists of five different dimers whose polypeptide chains are encoded by four

different genes. The PDGF chains PDGF-A, PDGF-B, PDGF-C and PDGF-D homo- or hetero-dimerize constituting the isoforms PDGF-AA, PDGF-BB, PDGF-AB, PDGF-CC and PDGF-DD. PDGF exerts its action through two specific receptor tyrosine kinases (RTKs), PDGF receptor (PDGFR) α and β. Ligand binding results in receptor dimerization and autophosphorylation, which triggers signal initiation at the plasma membrane. PDGFRα and PDGFRβ can again form homo- or heterodimers. Whereas PDGFRα homodimers are preferentially induced by PDGF-AA, PDGF-BB, PDGF-AB and PDGF-CC isoforms, PDGF-BB and PDGF-DD induce PDGFRβ homodimers. The heterodimer is thought to be induced by all isoforms except PDGF-AA [16]. Although both receptors activate similar signaling pathways and evoke mitogenic signals, PDGFRβ is the more potent in transducing cell motility [16,17]. For the termination of PDGF signaling, the ligand−receptor complex is internalized via clathrin−coated pits into endosomes, promoted by prior ubiquitination of the receptor molecules by members of the Cbl family of ubiquitin E3 ligases. Most of the receptors are degraded in lysosomes, however, recycling of the receptors can also be triggered under certain circumstances [18−21]. Dysregulation of PDGFR signaling is associated with several malignant processes, such as fibrosis and cancer development in concert with altered TGFβ signaling [22−25] or with the impairment of the wound healing process [26]. Although some features observed as part of the RDEB phenotype might be influenced by PDGFR, little is known about the role of PDGFR signaling in the pathogenesis of RDEB. In this study, we investigate whether the loss of C7 causes the dysregulation of PDGFRβ-mediated signaling in RDEB skin fibroblasts and its potential impact on their wound healing capacity in the dermis.

Results

Altered PDGFR-β signaling in RDEB fibroblasts

To study whether loss of C7 could lead to alterations in PDGFRβ signaling, we investigated tyrosine phosphorylation upon stimulation with PDGF-BB in primary normal human fibroblasts (NHF) and RDEB fibroblasts. To determine a suitable concentration of PDGF-BB which induces a robust, cell type-nonspecific activation of PDGFR supporting mass spectrometry (MS)-based proteomic analyses, we performed a dose-response analysis (**Supplementary Fig. S1**). 25 ng/mL of PDGF-BB induced a maximum of tyrosine phosphorylation in all tested cases and was used for subsequent MS experiments (see Experimental Procedures for details). Three different RDEB fibroblasts and NHFs each were stimulated with PDGF-BB for 0,

5 and 10 min and we observed that RDEB fibroblasts showed in general lower intensities of tyrosine phosphorylation compared to NHF (**Fig. 1A**), indicating an attenuation of PDGFR activity in RDEB.

To identify proteins being differentially phosphorylated after PDGF-BB stimulation, we quantified phosphotyrosine-containing proteins by stable isotope labeling by amino acids in cell culture (SILAC)-based MS analyses (**Fig. 1B**) (see Experimental Procedures). Biological replicates with SILAC-label swaps were analyzed to exclude unspecifically enriched proteins, contaminants and false-positive hits. In three biological replicates each, we identified 2'324 proteins in total. 156 proteins with a significant enrichment in at least one timepoint were used for the follow-up analysis (Significance A, FDR ≤ 0.05, BH corrected, **Supplementary Table S1**). For the significantly enriched proteins, the average ratios of biological replicates were *z*-normalized (ungrouped), and subjected to a *k*-means cluster analysis [27]. For NHF and RDEB each cluster contained the same set of proteins, allowing a direct comparison of cell types (**Fig. 1C**). Clusters 3 and 4 comprised proteins with a similar induction in tyrosine phosphorylation in NHF and RDEB fibroblasts. This cluster was associated with transmembrane receptor protein tyrosine-kinase signaling pathways and PDGFR as indicated by GO term analysis (Fisher's exact test, *p* < 0.05, BH-corrected). SILAC ratios of enriched PDGFRα and PDGFRβ revealed similar inductions in tyrosine phosphorylation in NHF and RDEB fibroblasts, the latter responding slightly weaker (**Supplementary Table S1**). Clusters 1 and 2 contained proteins that were early (cluster 2) or late (cluster 1) enriched in NHF upon PDGF-BB stimulation, but showed a reduced tyrosine phosphorylation induction in RDEB. These groups contained proteins associated with extracellular exosome, membrane-bounded organelles (cluster 1) as well as focal adhesion and adherens junction (cluster 2). Interestingly, cluster 5, which is associated with endocytosis, showed a clear induction of tyrosine phosphorylation after 5 and 10 min stimulation in RDEB fibroblasts, but no or significantly weaker induction in NHF (**Table 1**).

Levels of Cbl E3 ligases are increased in RDEB fibroblasts

Cluster 5 contained an interesting protein that can be linked to altered receptor tyrosine kinase (RTK) activity: c-Cbl (CBL, **Fig. 1C, Table 1**). It is an E3 RING ubiquitin ligase linked to ubiquitination and degradation of several RTKs upon growth factor stimulation, PDGFRβ being one of them [20]. In agreement with the cluster analysis, both c-Cbl and its homologue Cbl-b, which was only identified in RDEB cells, were significantly higher enriched in RDEB fibroblasts than in NHF after 5 min of PDGF-
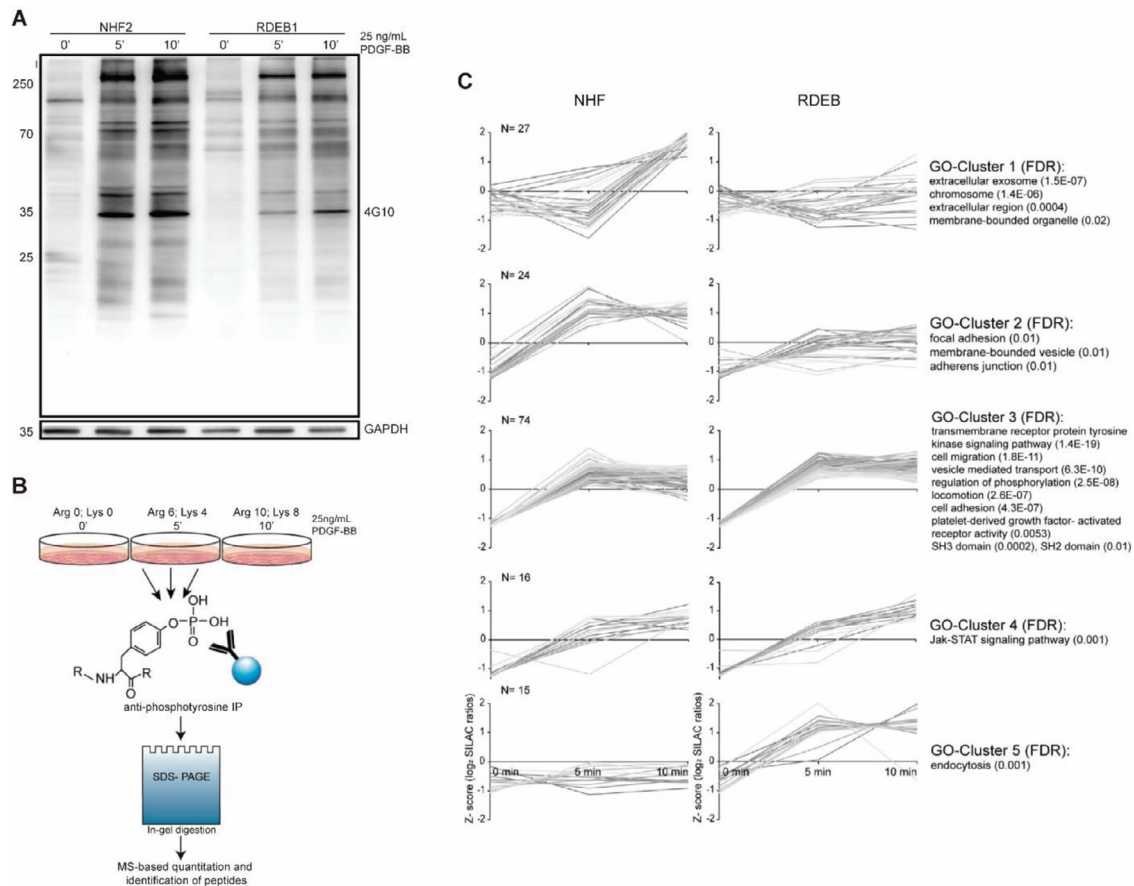
Fig. 1. RDEB fibroblasts present differential PDGFR signaling upon stimulation. (**A**) Western blot analysis of phosphotyrosine containing proteins in NHF and RDEB fibroblasts after stimulation with 25 ng/mL PDGF-BB for 5 and 10 min. (**B**) MS-based workflow of the quantitative analysis of PDGFR-based phosphotyrosine signaling. Each cell type was subjected to three different SILAC labels and stimulated with PDGF-BB. Unstimulated cells were used as controls. Three different NHF (NHF2, 4, 8) and RDEB (RDEB1, 4, 5) cells were analyzed. Anti-phosphotyrosine immunoprecipitated samples were in-gel digested and analyzed by LC-MS/MS. (**C**) Cluster analysis of significantly enriched proteins after phosphotyrosine-IP. MS-data of significantly enriched proteins (BH-corrected FDR ≤ 0.05) was *z*-normalized and *k*-means clustered: protein profiles of NHF are shown on the left and RDEB fibroblasts on the right. GO-term enrichment of the proteins in each cluster was computed with a FDR ≤ 0.05 (respective *p*-values are noted in brackets) and a minimum of four proteins per GO-term had to be annotated.

BB stimulation (**Fig. 2A**). Thus, phosphorylated levels of these proteins were higher in RDEB fibroblasts upon growth factor stimulation, which points to an elevated activity of them [19,20]. Also by western blot analysis, c-Cbl and Cbl-b were more enriched in phosphotyrosine immunoprecipitations in RDEB fibroblasts stimulated by PDGF-BB (**Fig. 2B**), confirming that RDEB fibroblasts present increased phosphorylated levels of c-Cbl and Cbl-b after PDGFR stimulation.

To test whether the increase of c-Cbl and Cbl-b observed by LC-MS/MS and western blot is due to an increase in their phosphorylation or their abundance, we analyzed whole cell lysates of RDEB fibroblasts and NHF. Interestingly, RDEB fibroblasts presented higher protein levels of Cbl-b and c-Cbl (**Fig. 2C**), indicating that the higher phosphorylation

levels are due to a dysregulation of Cbl protein abundance and not PDGFR activity. This agrees to the observation that PDGFR itself was not substantially dysregulated in RDEB fibroblasts compared to NHF (**Supplementary Table S1**). Altogether, these results indicate that RDEB fibroblasts present elevated levels of c-Cbl and Cbl-b that, upon PDGF-BB stimulation, become activated through phosphorylation, which might affect PDGFRβ activity in RDEB fibroblasts.

Rapid internalization and degradation of PDGFRβ upon stimulation in RDEB fibroblasts

Cbl E3 ubiquitin ligases are implicated in negative regulation of RTKs by inducing their ubiquitination and subsequent degradation [20]. To study if

Table 1. Proteins enriched in phosphotyrosine affinity purifications in RDEB cells. Proteins were more enriched in RDEB fibroblasts compared to NHF (cluster 5 in Fig. 1; see supplementary Table S1 for more details). Shown are normalized SILAC ratios and numbers of identified peptides per protein. Multiple gene names are listed in case peptides could not discriminate between respective proteins.

Gene names	Protein IDs	Number of peptides	NHF			RDEB		
			0 min	5 min	10 min	0 min	5 min	10 min
ACOT13	Q9NPJ3	2	1.00	0.95	0.90	1.00	3.41	0.81
ACTA2;ACTG2	P62736;P63267	34	1.00	1.10	1.38	1.00	2.65	2.33
CALCOCO2	Q13137	4	1.00	0.94	1.26	1.00	3.17	4.07
CBL	P22681	6	1.00	1.00	0.96	1.00	13.95	6.79
CDC42	P60953	10	1.00	2.00	1.94	1.00	5.22	6.24
EIF3G	O75821	6	1.00	0.94	0.88	1.00	1.22	2.83
EPN2	O95208	3	1.00	1.82	1.93	1.00	5.22	7.20
FAM129A	Q9BZQ8	8	1.00	1.00	0.97	1.00	2.63	2.29
KDELC2	Q7Z4H8	6	1.00	0.47	0.56	1.00	2.98	2.63
KRT18	P05783	12	1.00	0.60	0.73	1.00	2.94	3.32
PCDHGA10	Q9Y5H3	8	1.00	3.15	2.34	1.00	17.04	12.48
RAB13	P51153	8	1.00	1.81	1.95	1.00	5.28	5.74
RAD23B	P54727	11	1.00	0.98	1.08	1.00	1.56	2.68
RHOA	P61586	7	1.00	1.44	1.56	1.00	3.07	3.59
YTHDF3;YTHDF1	Q7Z739;Q9BYJ9	5	1.00	1.13	1.02	1.00	2.84	3.31
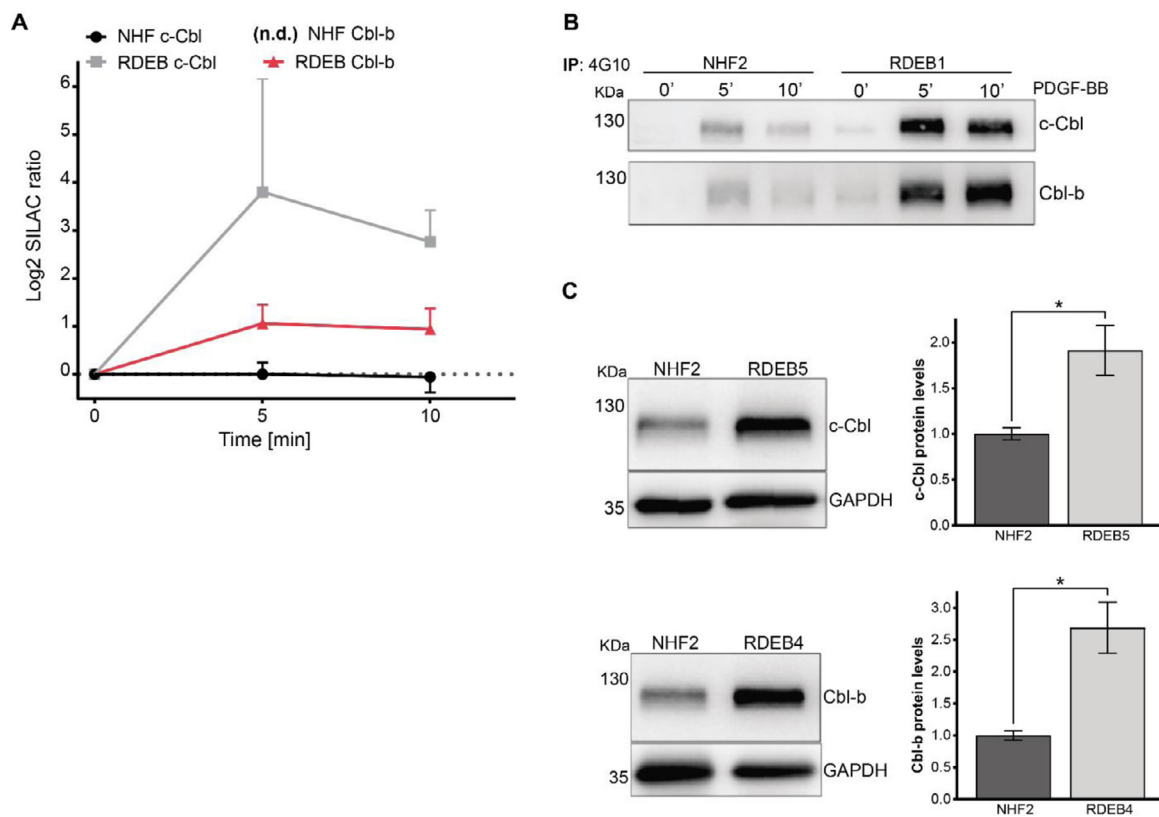
Fig. 2. Abundance of Cbl E3 ubiquitin ligases is increased in RDEB fibroblasts. (**A**) Log$_2$SILAC ratios of c-Cbl and Cbl-b, proteins identified in cluster 5, extracted from the cluster analysis obtained from LC-MS/MS experiments represented in Fig. 1C. n.d. = not detected. (**B**) Representative western blot of Cbl-b and c-Cbl after anti-phosphotyrosine IP of NHF and RDEB fibroblasts stimulated with 25 ng/mL PDGF-BB for the indicated timepoints. (**C**) Western blot and quantification of Cbl-b and c-Cbl levels in whole cell lysates of NHF and RDEB fibroblasts. Data are represented as mean $\pm$ s.e. ($n = 3$), * $p \leq 0.05$ using Student's t-test for the comparison between NHF and RDEB fibroblasts.

elevated levels of Cbl-b in RDEB fibroblasts affect the half-life of PDGFRβ, fibroblasts were stimulated with PDGF-BB for different timepoints and PDGFRβ levels were analyzed. We found that 5 min treatment

with PDGF-BB led to practically complete degradation of the receptor in RDEB fibroblasts, while in NHF we only observed approximately 50% degradation (**Fig. 3A**). Since PDGFRβ ubiquitination by the aforementioned E3 ligases is the signal for degradation, we investigated ubiquitination levels of the receptor upon growth factor stimulation. NHF and RDEB fibroblasts were subjected to a 3 min treatment with 15 ng/mL PDGF-BB and PDGFRβ was immunoprecipitated for analyzing ubiquitination levels. Indeed, RDEB fibroblasts presented up to 4-times higher ubiquitination levels of PDGFRβ than NHF (**Fig. 3B**). Moreover, we again observed a rapid degradation of PDGFRβ in RDEB fibroblasts, since PDGFRβ levels were reduced upon 3 min stimulation, while in NHFs there was no reduction (**Fig. 3B**, left bottom panel).

To study PDGFRβ internalization upon PDGF-BB stimulation, we also performed immunofluorescence microscopy and analyzed its co-localization with sortin nexin-1 (SNX1), an endosomal protein described to play a role in sorting RTKs to lysosomes for their degradation upon growth factor stimulation [28,29]. NHF and RDEB fibroblasts were treated for 5 min with 15 ng/mL PDGF-BB and co-immunostained for PDGFRβ and SNX1. Upon stimulation, the receptor was internalized in both cell types changing to a more punctuate, cytoplasmic pattern (**Fig. 3C**, PDGFRβ panels). Likewise, SNX1 puncta presence increased in the cytoplasm of PDGF-treated cells, being more intense in RDEB fibroblasts (**Fig. 3C**, SNX1 panels). Co-localization between SNX1 and PDGFRβ was observed in both cell types, indicating that receptor molecules were directed to lysosomes for degradation, but to a significantly greater extent in RDEB (**Fig. 3C**, Merge panel and bottom panel), indicating that the degradation process is faster in these cells. Collectively, these results indicate that, upon PDGF-BB stimulation, PDGFRβ is more rapidly ubiquitinated, internalized and degraded in RDEB fibroblasts likely due to the presence of higher levels of Cbl E3 ligases.

RDEB fibroblasts present an attenuated response to PDGF-BB stimulation

To study whether faster PDGFRβ degradation in RDEB fibroblasts influences its downstream signaling, we investigated potential effects in two central pathways regulated by PDGFRβ: the mitogen-activated protein kinase/extracellular signal-regulated kinases (MAPK/ERK) pathway [30,31] and the phosphatidylinositol 3-kinase (PI3K)/AKT pathway [32,33]. NHF and RDEB fibroblasts were subjected to up to 8 h of PDGF-BB stimulation and phosphorylated ERK1/2 and AKT levels were analyzed. We found that in both cell types PDGFRβ activation led to the phosphorylation of ERK1/2 and AKT, but in

NHF the signal was more stable and lasted longer than in RDEB cells (**Fig. 4A**).

It is known that MAPK and PI3K/AKT signaling regulate different cellular processes, such as proliferation or cell motility, which are important in wound healing [30,33]. Given our previous results and the described impairment of the wound healing process in RDEB [34], we investigated cell proliferation upon PDGF-BB stimulation. RDEB fibroblasts showed significantly diminished proliferation compared to NHF, both in basal conditions and after growth factor stimulation (**Fig. 4B**). Importantly, whereas NHF showed a significant increase in cell proliferation after PDGF-BB stimulation, RDEB fibroblasts responded weaker, in a non-significant manner. Next, we performed a scratch assay for studying cell motility. After inflicting the scratch, NHF and RDEB fibroblasts were treated with vehicle or PDGF-BB and cell migration was followed for 30 h. In order to block cell proliferation, fibroblasts were treated with mitomycin C in all assayed conditions. We found that cell motility was also affected in RDEB fibroblasts both in basal conditions and after PDGF-BB stimulation. Although the migration rate increased in response to PDGF-BB, RDEB fibroblasts never reached the migration levels of NHFs (**Fig. 4C**). Taken together, these results indicate that RDEB fibroblasts are capable of responding to PDGF-BB stimulation; however, their response is impaired compared to NHFs, with different kinetics of ERK and AKT activation and lower proliferative and migratory capacities.
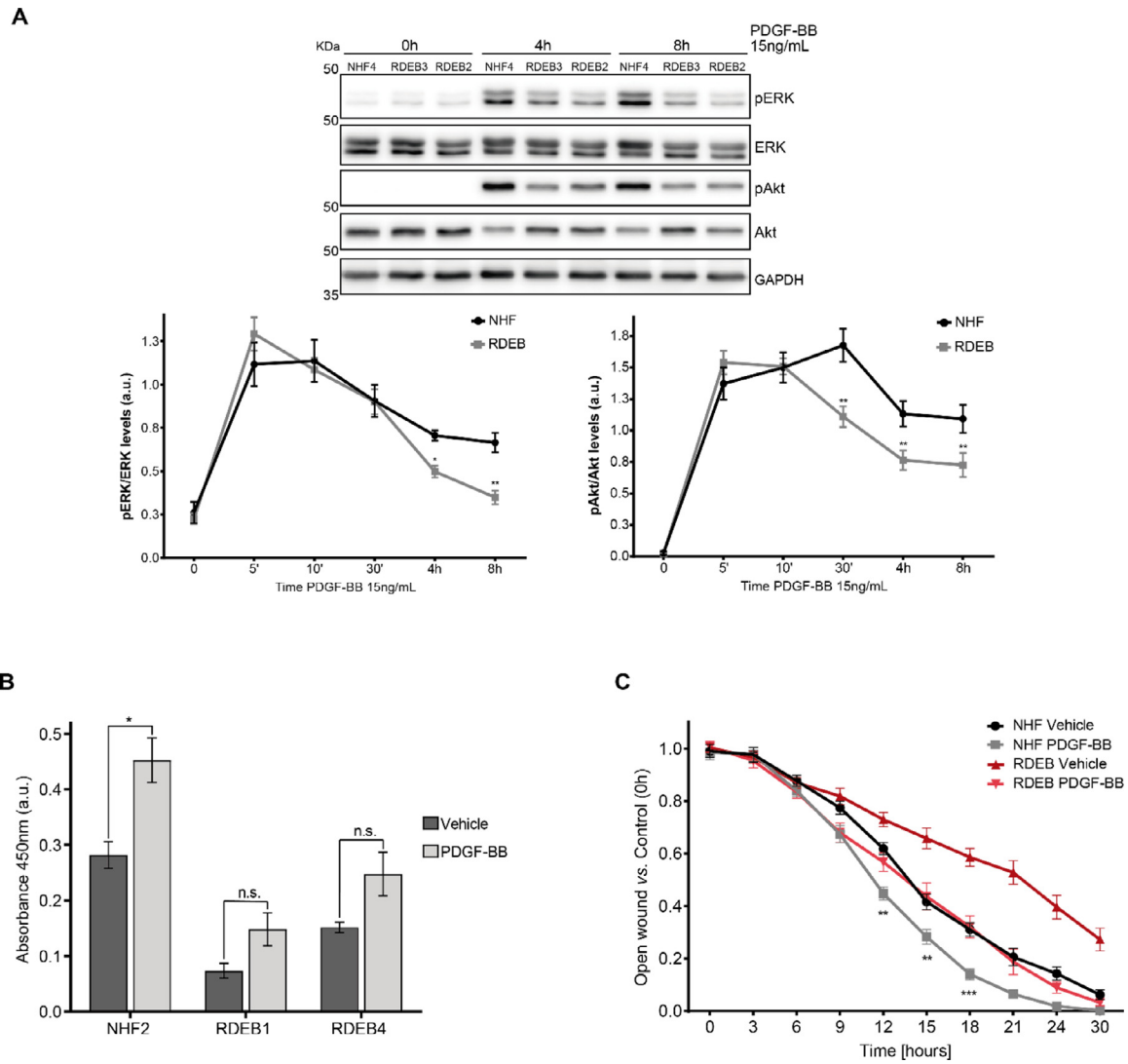
Altered TGFβ signaling in RDEB fibroblasts induces elevated Cbl levels

In RDEB, increased TGFβ receptor signaling is considered as one of the main pathways implicated in impairment of wound healing and in maintaining a characteristic, inflammatory, fibrotic microenvironment [35−37]. As TGFβ stimulation was shown amongst others to lead to an increase in c-Cbl expression in mouse fibroblasts [38], we tested if increased TGFβ levels might be the cause for elevated Cbl-b protein levels in RDEB fibroblasts. We verified that Cbl-b levels were increased in a time-dependent manner upon TGFβ stimulation in NHF (**Fig. 5A, B**), suggesting that elevated levels of Cbl-b in RDEB fibroblasts could be caused by the upregulation of TGFβ signaling. Phosphorylation of Smad3, a well-known target of the TGFβ pathway, was used as a readout for an effective activation of the receptor (**Fig. 5A**).

As TGFβ signaling is constitutively activated in RDEB, we blocked it in RDEB fibroblasts with LY210976, a TGF-β receptor type I/II (TβRI/II) dual inhibitor. Indeed, Cbl-b levels were downregulated after 24 h of LY210976 treatment, reaching similar levels as observed in NHF (**Fig. 5C, D**). Again,
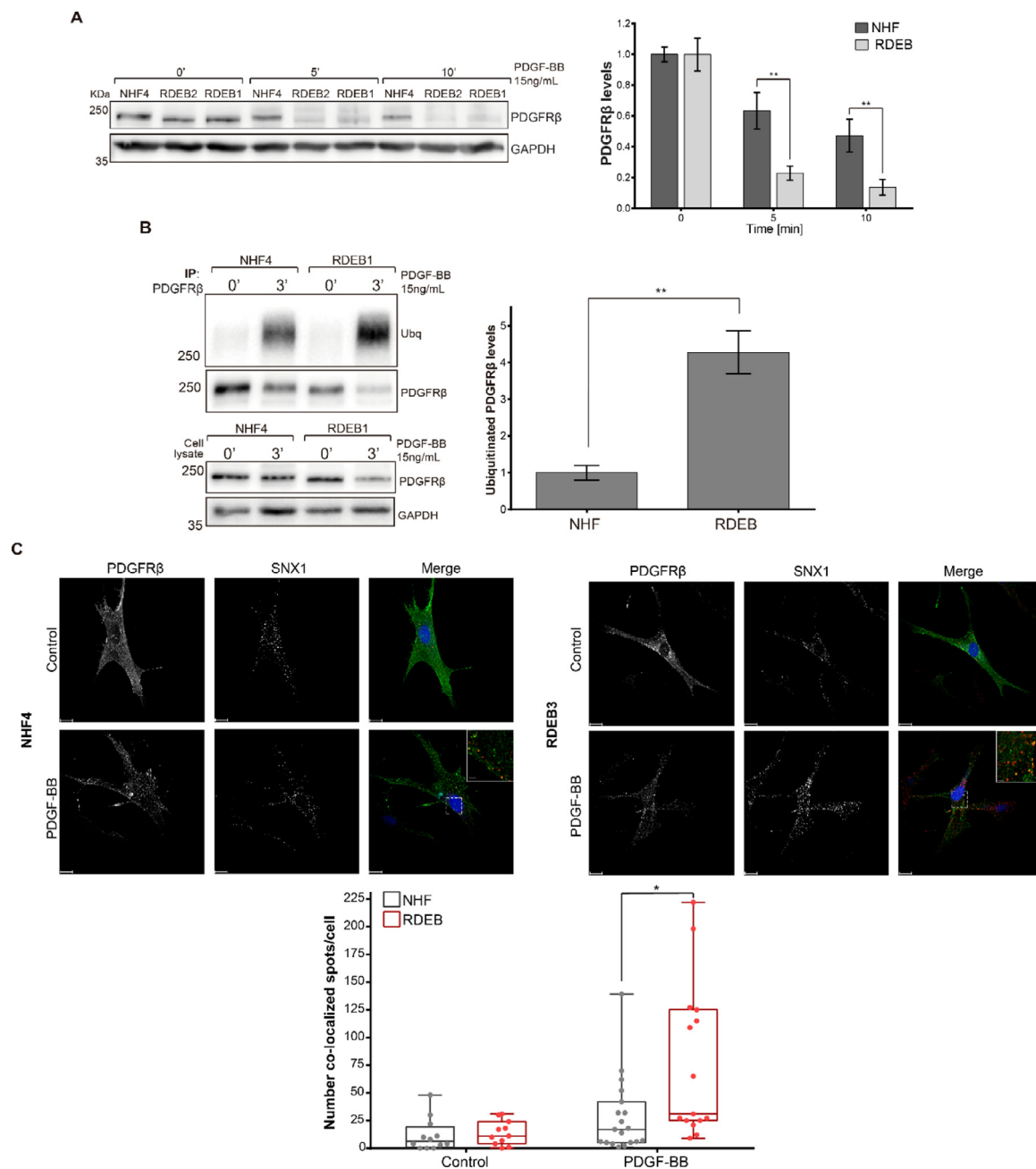
Fig. 3. Increased PDGFRβ degradation upon growth factor stimulation in RDEB fibroblasts. (A) Representative western blot (left panel) and quantification of PDGFRβ levels (right panel) in NHF and RDEB fibroblasts in control conditions and after stimulation with 15 ng/mL PDGF-BB for the indicated timepoints. Data was normalized to GAPDH levels. Comparisons were performed between NHF and RDEB cells at the respective timepoints. Data are represented as mean ± s.e. (n = 3), including two different NHF (NHF4, 9) and three RDEB (RDEB1-3) types in each experiment. **$p \leq 0.01$ using Student's t-test computed with a FDR ≤ 0.05 for multiple testing. **(B)** Representative western blot (left panel) and quantification (right panel) of PDGFRβ ubiquitination after 3 min of stimulation with 15 ng/mL PDGF-BB. PDGFRβ was immunoprecipitated prior ubiquitin detection. Corresponding whole cell lysates were analyzed. Ubiquitinated levels were normalized to the corresponding levels of immunoprecipitated PDGFRβ. Data are represented as mean ± s.e. (n = 3), including two different NHF (NHF4, 9) and three RDEB (RDEB1-3) types in each experiment. **$p \leq 0.01$ using Student's *t*-test for the comparison between NHF and RDEB fibroblasts. **(C)** Representative image (upper panel) and quantification (bottom panel) of immunofluorescence analysis of PDGFRβ/SNX1 co-localization. NHF and RDEB cells were stimulated 5 min with 15 ng/mL PDGF-BB. Cells were co-immunostained with specific anti-PDGFRβ (green) and anti-SNX1 (red) antibodies and analyzed by confocal microscopy. Nuclei were stained with Hoechst 33258 (blue). Scale bars, 15 μm. Insets = higher magnification of the relative areas within the white-dotted boxes. Scale bars, 2 μm. Quantification was performed by object-based co-localization extension with Imaris software. Data represented in box plot showing the number of co-localized PDGFRβ/SNX1 spots per cell in each condition. Between 15 and 19 cells were counted per condition, each of them including two NHF (NHF4, 9) and two RDEB (RDEB 2-3) cell types. *$p \leq 0.05$ using Student's *t* test computed with a FDR ≤ 0.05 for multiple testing.

Fig. 4. Attenuated PDGF-induced downstream signaling in RDEB fibroblasts compared to NHF. (A) Representative western blot (upper panel) and quantification (bottom panel) of phosphorylated ERK1/2 (pERK) and Akt (pAkt) levels after stimulation with 15 ng/mL PDGF-BB at the indicated timepoints. Data were normalized to GAPDH and total ERK1/2 (pERK/ERK) or Akt (pAkt/Akt). Data are represented as mean $\pm$ s.e. ($n = 3$) each experiment including two different NHF (NHF4, 9) and three RDEB (RDEB1-3) cell types. *$p \leq 0.05$, **$p \leq 0.01$ using Student's t-test computed with a FDR ≤ 0.05 for multiple testing. **(B)** BrdU cell proliferation assay was performed in NHF and RDEB fibroblasts treated with vehicle or 25 ng/mL PDGF-BB for 24 h. Data are represented as mean $\pm$ s.e. ($n = 3$), *$p \leq 0.05$, n.s. = non-significant using a two-way ANOVA with a Holm-Sidak test post hoc analysis. Note: values of NHF and RDEB cells were significantly different in all conditions, $p \leq 0.05$. **(C)** NHF and RDEB fibroblasts were subjected to scratch assays in presence of 1 μg/mL of mitomycin *C*. Cells remained untreated (vehicle) or treated with 5 ng/mL PDGF-BB. The motility of cells was monitored by time-lapse video microscopy (Incucyte® Live Cell analysis system, Essen Biosciences) and wound closure quantification was performed with ImageJ (NIH) software. NHF and RDEB data was normalized to their respective control (0 h). Data are represented as mean $\pm$ s.e. ($n = 3$) each experiment including two different NHF (NHF4, 9) and RDEB (RDEB1, 2) cells. Statistical comparisons were made between NHF and RDEB stimulated with PDGF-BB at the respective timepoints. **$p \leq 0.01$ and ***$p \leq 0.001$ using two-way ANOVA with a Tukey test post hoc analysis.

phosphorylated Smad3 was used as readout of effective blockade of the receptor (**Fig. 5C, E**). Interestingly, basal levels of phosphorylated Smad3 seemed to be similar in NHF and RDEB fibroblasts; however, we noticed that the proportion of

phosphorylated Smad3 was significantly higher in RDEB fibroblasts as total Smad3 levels were lower in these cells (**Fig. 5E**). We hypothesized that the observed differences in Smad3 levels between cell types could be due to problems in solubilizing

nuclear, DNA-bound Smad3 [39]. Supporting this hypothesis, we did observe increased nuclear localization of Smad3 in RDEB fibroblasts by fluorescence microscopy in agreement with activated TGFβ signaling in RDEB (**Supplementary Fig. S2**).

To study whether Cbl-b levels were transcriptionally regulated by the TGFβ pathway we performed qRT-PCR. NHF and RDEB fibroblasts were treated for 6 h with 5 μM LY210976 or vehicle and *CBLB* mRNA expression levels were measured. *HPRT1* (Hypoxanthine Phosphoribosyltransferase 1) was used as control. We verified that, at basal conditions, RDEB fibroblasts presented higher expression levels of *CBLB* than NHF and that TGFβ receptor blockade with LY210976 decreased *CBLB* mRNA levels (**Fig. 5F**). To further demonstrate that *CBLB* expression was induced by TGFβ, we treated NHF with 10 ng/mL TGFβ and/or 5 μM LY210976, measured *CBLB* mRNA levels and corroborated that TGFβ induces *CBLB* transcription. Blockade of this signaling pathway prevents the increase in *CBLB* mRNA levels, verifying that changes are pathway specific (**Fig. 5G**).

Collectively, these results indicate that elevated levels of Cbl-b in RDEB fibroblasts are caused by the upregulation of TGFβ signaling, which induces *CBLB* transcription, and that blocking this signal leads to a decrease in the levels of Cbl-b E3 ubiquitin ligase (**Fig. 6**).

Discussion

PDGFRβ signaling is crucial for fibroblast homeostasis and regulates diverse processes such as wound healing and fibrosis [16,22,40−42], both of which are dysregulated in RDEB [6,8,34]. However, little is known about PDGFR signaling in RDEB and its potential role in wound healing and fibrosis upon loss of C7. Here, we present data that elevated TGFβ signaling due to the loss of C7 affects PDGFRβ signaling and how this impairs processes related to wound healing, i.e. cell proliferation and migration.

Employing an unbiased phosphoproteomic approach, we observed overall attenuated PDGFRβ signaling upon PDGF-BB treatment in RDEB fibroblasts. In total 51 proteins responded in NHF but not in RDEB fibroblasts to PDGF-BB stimulation. Respective proteins were associated with GO terms related to the extracellular region and molecular mechanisms associated with the cell membrane, such as ECM-receptor interaction, focal adhesions and membrane-bound vesicles, in accordance with the fact that RDEB fibroblasts present alterations in the ECM, which provokes changes in cell-ECM interactions [37]. Of note, we found two members of the Cbl family of RING finger-containing E3 ubiquitin ligase, c-Cbl and Cbl-b, to not follow this trend and

to be increasingly phosphorylated in RDEB fibroblasts.

Cbl E3 ligases are important negative regulators of RTKs. They are activated by tyrosine phosphorylation after growth factor stimulation and induce ubiquitination, internalization and degradation of RTKs [19,20]. Our data show that RDEB fibroblasts not only present higher levels of phosphorylated c-Cbl and Cbl-b upon PDGF-BB stimulation compared to NHF, but that they have increased overall levels of these proteins. Therefore, one might predict that attenuated PDGFRβ signaling in RDEB fibroblasts could be caused by enhanced levels of Cbl E3 ligases, which provoke a prompt downregulation of the receptor upon PDGF-BB stimulation, leading to reduced signal transduction. Our results showed that, upon PDGF-BB stimulation, PDGFRβ is more rapidly ubiquitinated, internalized and degraded in RDEB compared to normal fibroblasts, which agrees with observations that high ubiquitination levels encode efficient RTK degradation [43]. Interestingly, we observed a rapid degradation in both cell types, the majority of PDGFRβ being degraded within 10 min. If this is a general phenomenon in skin fibroblasts or due to the chosen experimental conditions will have to be addressed in future studies. Analysis of ERK1/2 and AKT phosphorylation, two of the main pathways regulated by PDGFRβ related to mitogenic signaling and cell motility [30,32], revealed that in RDEB fibroblasts the signaling extinguishes earlier compared to NHF upon PDGF-BB stimulation. This result verified that the more rapid degradation of PDGFRβ in RDEB after its activation leads to reduced signal transduction. Nonetheless, despite the rapid degradation of PDGFR upon stimulation, we observed that ERK1/2 remains active up to 8 h after the treatment. This effect is in line with previous reports describing sustained activation of ERK by PDGF, contrary to the rapidly extinguished signaling triggered by EGF. The former appears necessary for activation of proliferation of quiescent fibroblasts [44,45].

To explore whether the differences in ERK and AKT signaling led to differences in cell responses, we analyzed cell proliferation and motility in PDGF-BB stimulated fibroblasts. Both processes are tightly related with wound healing. As expected, RDEB fibroblasts presented less proliferative and migratory capacities in basal conditions when compared to NHF. Nonetheless, RDEB fibroblasts were capable of responding to PDGF-BB, since we observed an increase in proliferation and migration rates after stimulation; however, their proliferative and migratory capacities were always lower than the ones of NHF. These results reinforce the hypothesis that the response triggered in RDEB fibroblasts after PDGFRβ activation is abnormal.

Since it was reported that increased TGFβ activity induces the expression of c-Cbl in mice [38], and
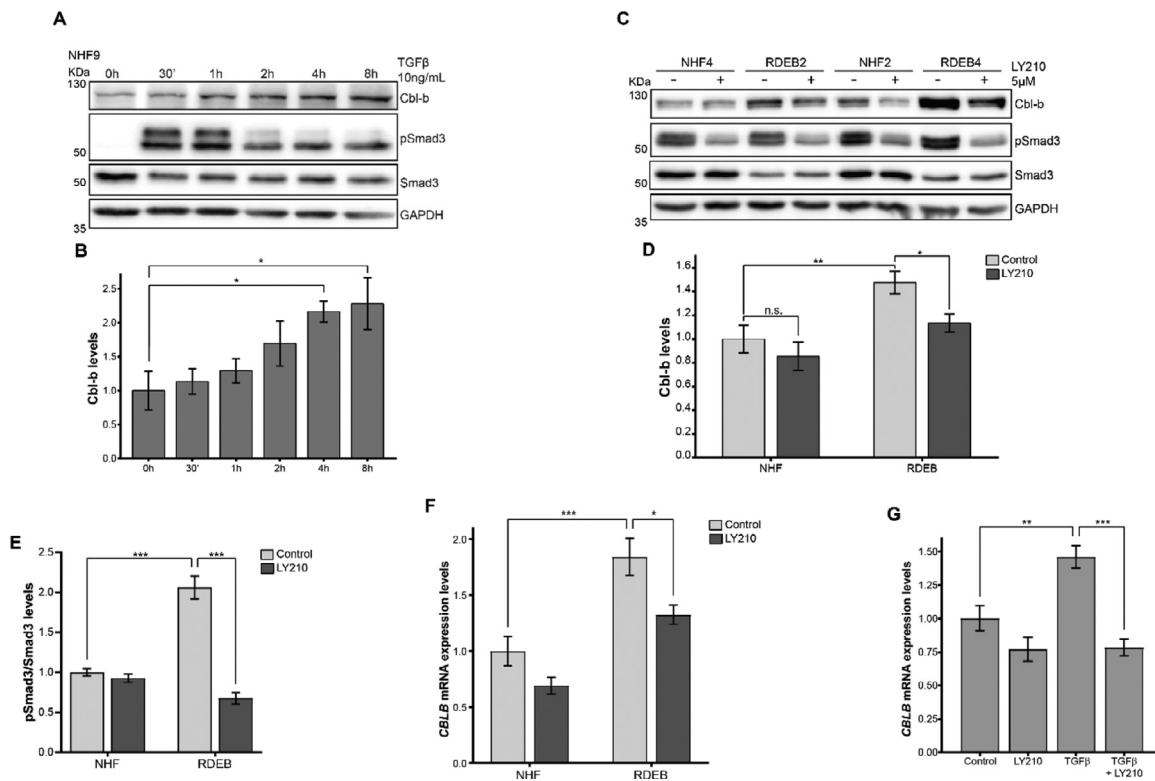
Fig. 5. TGFβ regulates the differential expression of Cbl-b E3 ubiquitin ligase in RDEB fibroblasts. (A) Representative western blot of Cbl-b and phosphorylated Smad3 (pSmad3) levels and **(B)** quantification of Cbl-b levels in NHF subjected to 10 ng/mL TGFβ treatment at different timepoints. Data were normalized to GAPDH. Data are represented as mean ± s.e. (*n* = 3) each experiment including two different NHF (NHF4, 9). Statistical comparison was made with respect the control (0 h). *$p \leq 0.05$ using one-way ANOVA with a Dunnet test post hoc analysis. **(C)** Representative western blot and **(D)** quantification of Cbl-b levels upon TGFβ signaling blockade with LY210976 (LY210, 5 μM for 24 h). Data were normalized to GAPDH and are represented as mean ± s.e. (*n* = 3) including three different NHF (NHF2, 4, 9) and three RDEB (RDEB2, 3, 4) cell types. * $p \leq 0.05$ and **$p \leq 0.01$ using Student's t-test. n.s. = non-significant. **(E)** Quantification of pSmad3 compared to Smad3 levels upon TGFβ signaling blockade with LY210976 (LY210, 5 μM for 24 h). Data were normalized to GAPDH and are represented as mean ± s.e. (*n* = 3) including three different NHF (NHF2, 4, 9) and three RDEB (RDEB2, 3, 4) cell types. ***$p \leq 0.01$ using two-way ANOVA with a Tukey test post-hoc analysis. **(F)** *CBLB* mRNA levels in NHF and RDEB fibroblasts upon TGFβ receptor signaling blockade with LY210976 (LY210, 5 μM for 6 h). Data were normalized to *HPRT1* levels and are represented as mean ± s.e. (*n* = 3) including three different NHF (NHF2, 4, 8) and three RDEB (RDEB2, 3, 4) cell. * $p \leq 0.05$ and ***$p \leq 0.001$ using two-way ANOVA with a Tukey test post-hoc analysis. **(G)** *CBLB* mRNA levels in NHF subjected to 10 ng/mL TGFβ prior blockade with LY210976 (LY210, 5 μM for 4 h). Data were normalized to *HPRT1* levels and are represented as mean ± s.e. (*n* = 3) including three different NHF (NHF2, 4, 8). * $p \leq 0.05$ and ***$p \leq 0.001$ using one-way ANOVA with a Tukey test post-hoc analysis.

TGFβ signaling is upregulated in RDEB, being one of the most important modulators of this disease [34,37,46], we investigated whether TGFβ upregulation might induce the increase in Cbl protein levels. Our data support this hypothesis, since activation of TGFβR in NHF led to an increase of *CBLB* expression both at transcriptional and protein level. Moreover, blocking TGFβ signaling with a pharmacological inhibitor in RDEB fibroblasts led to a decrease in Cbl-b levels, strengthening the aforementioned hypothesis. The mechanism by which TGFβ induces *CBLB* expression remains to be determined and is an active topic of our current investigations.

Taken together, our data show that increased TGFβ signaling occurring in RDEB fibroblasts induces an increase in levels of the E3 ubiquitin ligase Cbl-b. This leads to attenuated PDGFRβ signaling due to a more rapid internalization and degradation upon PDGF-BB stimulation, which in turn provokes a more rapid extinction of downstream signaling and, subsequently, limited cellular responses, such as proliferation and cell motility, key processes for proper wound healing (Fig. 6). Loss of C7 induces numerous alterations in ECM and cell homeostasis apart from the explored ones, known and unknown, that may act as disease modifiers and might contribute to aberrant ERK signaling. Thus, further work is

necessary to fully understand the role of PDGFRβ and other disease modifiers in the dynamic processes of healing and fibrosis in RDEB. This study provides new understanding of the molecular and cellular pathogenesis of RDEB and consequently new insights into potential therapy options. In the clinic, PDGF-BB has been topically applied to enhance the healing of chronic wounds and loss of myofibroblast features in a MAPK dependent manner [47,48]. However, in the light of our findings, this treatment might not be efficient in RDEB due to chronically increased activation of TGFβ signaling.

Experimental procedures

Primary skin cells culture

Normal human primary fibroblasts (NHF) were isolated from the foreskin of circumcised 2-, 4-, 8- and 9-year old healthy boys. Primary dermal fibroblasts from RDEB patients were obtained from skin specimens of 6 different donors who were less than one year of age [37,49]. RDEB fibroblasts used in this study were selected based on the absence of C7 as detected by Western blotting. The study was approved by the Ethics Committee of Freiburg University (# 45/03-110631) and conducted according to the Declaration of Helsinki.

Fibroblasts were cultured in DMEM with 4.5 g/L glucose, L-glutamine and sodium pyruvate (PAN-Biotech, Aidenbach, Germany) supplemented with 10% fetal bovine serum (FBS) (ThermoFisher Scientific, Waltham, MA) and 1% Penicillin/Streptomycin (PAN-Biotech, Aidenbach, Germany) and maintained at 37 °C in a 5% CO2-humidified atmosphere. Cells were harvested with trypsin/EDTA solution (0.05%/0.02% weight/volume) (PAN-Biotech, Aidenbach, Germany). For quantitative analysis of proteins by mass-spectrometry, fibroblasts were SILAC-labeled. Cells were cultured in high-glucose SILAC-DMEM (Thermo Fisher Scientific) supplemented with 10% dialyzed fetal bovine serum (ThermoFisher Scientific, Waltham, MA), 1% Glutamax supplement (ThermoFisher Scientific), 1% Penicillin/ Streptomycin (PAN-Biotech) and 42 mg/L of L-arginine and 73 mg/L of L-lysine (Sigma). To reduce the arginine-to-proline conversion, 82 mg/L of L-proline was added to the media. Per experimental setup, the media was either supplemented with L-lysine-^{2}H$_4$ and L-arginine-^{13}C$_6$-^{14}N$_4$ (named as Lys4, Arg6) (Sigma-Aldrich, St. Louis, MO), L-lysine-^{13}C$_6$-^{15}N$_2$ and L-arginine-^{13}C$_6$-^{15}N$_4$ (named as Lys8, Arg10) (Sigma-Aldrich) or L-lysine and L-arginine (named as Lys0, Arg0) (Sigma-Aldrich). Fibroblasts were maintained in SILAC media for two weeks prior the performance of the experiments to ensure full amino acid labeling.

Reagents

Recombinant human platelet-derived growth factor-BB (PDGF-BB) and recombinant human transforming Growth Factor-β1 (TGFβ1; HEK293 derived) were purchased from PeproTech (Hamburg, Germany) and they were dissolved in sterile ddH$_2$O. TGFβ receptor inhibitor LY2109761 was purchased from MedChem Express (Monmouth Junction, NJ, USA) and it was resuspended in sterile dimethylsulfoxid (DMSO; Sigma-Aldrich). Primary antibodies anti-PDGFRβ (D-6; sc-374573), anti-ubiquitin (A-5; sc-166553) and GAPDH (FL-335; sc-25778) were purchased from Santa Cruz Biotechnologies (Heidelberg, Germany). Anti-phospho-Smad3 (S423 + S425) (EP823Y; ab52903) and anti-Smad3 (ab28379) were purchased from Abcam (Cambridge, UK). Antibodies anti-phospho-ERK 1/2 (T202/Y204) (#9101), anti-ERK 1/2 (#9102), anti-phospho-Akt (Ser473) (#9271), anti-Akt (#9272), PDGFRβ (28E1; #3169), anti-Cbl-b (D3C12; # 9498), anti-c-Cbl (D4E10; # 8447) were purchased from Cell Signaling Technology (St Louis, MO, USA). Anti-phosphotyrosine antibody conjugated to agarose beads (clone 4G10; 16-101) and anti-phosphotyrosine antibody (Clone 4G10; 05-321) were obtained from Merck Millipore (Darmstadt, Germany). Anti-SNX1 (Clone 51; 611482) antibody was purchased from BD Transduction Laboratories (BD Biosciences, Breda, The Netherlands). Horseradish peroxidase (HRP)-conjugate secondary antibodies anti-rabbit (111-035-045), anti-mouse (115-035-062) and anti-mouse light chain specific (115-035-174) were purchased from Jackson ImmunoResearch Laboratories (Newmarket, UK). Alexa Fluor 488 anti-rabbit and Alexa Fluor 594 anti-mouse were purchased from Invitrogen Life Technologies.

Phosphotyrosine enrichment by immunoprecipitation

Fibroblasts were serum-starved overnight prior to stimulation with 25 ng/mL of PDGF-BB for 0, 5, or 10 min. Cells were lysed in Triton buffer (50 mM Tris-HCl pH 7.4, 1% Triton-X 100, 137 mM NaCl, 1% Glycerine; Sigma-Aldrich) supplemented with phosphatase and protease inhibitors (cOmplete™ Protease Inhibitor Cocktail and PhosSTOP™; Roche, Rotkreuz, Switzerland). Cells were lysed for 2 h on ice. The protein concentration was determined by pierce BCA protein assay kit (ThermoFisher Scientific) and lysates were mixed in a 1:1:1 protein ratio. For the immunoprecipitation of phosphotyrosine-containing proteins, lysates were incubated with 75 μg of anti-Phosphotyrosine antibody conjugated to agarose beads (clone 4G10) for 4 h at 4 °C. After immunoprecipitation, the beads were washed with lysis buffer and proteins were eluted in 2x Laemmli loading buffer containing 1 mM
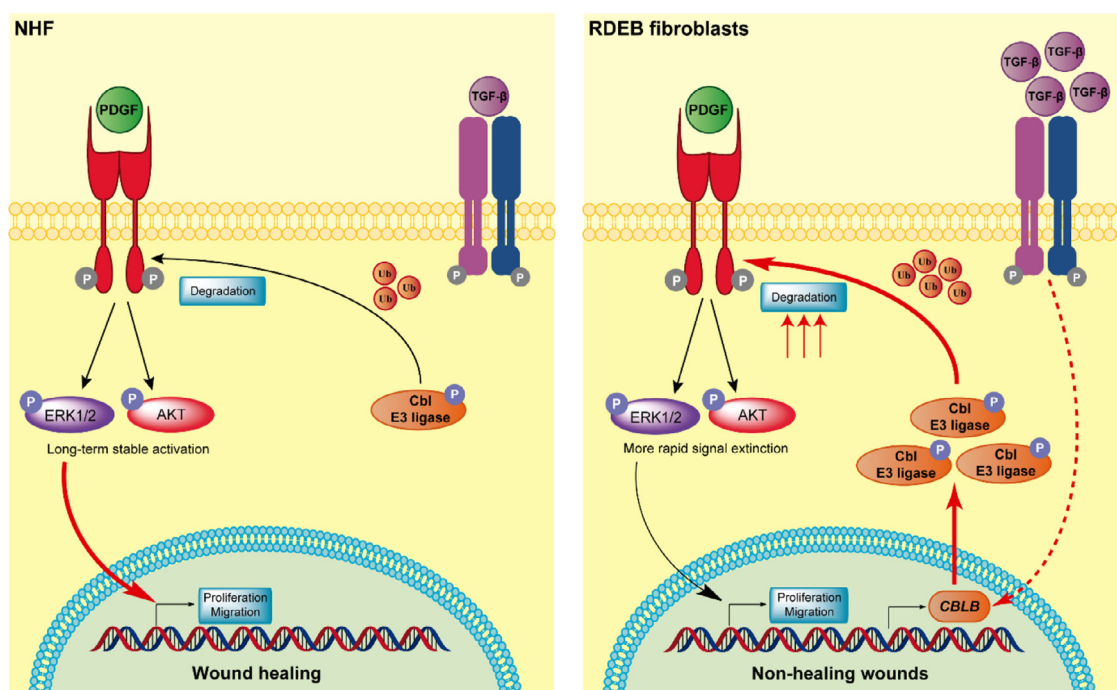
Fig. 6. Proposed mechanisms. In RDEB, increased TGFβ signaling compared to control conditions induces an increase in transcription and in protein levels of E3 ubiquitin ligases c-Cbl and Cbl-b. This leads to a more rapid ubiquitination, internalization and degradation PDGFRβ upon PDGF-BB stimulation, which in turn provokes a more rapid extinction of the downstream signaling and, subsequently, limited cellular responses, such as proliferation and cell motility, key processes for proper wound healing.

dithiothreitol (DTT; Amresco, Solon, OH) for 30 min. at 75 °C.

MS-based analysis of phosphotyrosine signaling events

After immunoprecipation of phosphotyrosine-containing proteins as described above, the reduced samples were alkylated with 5.5 mM iodoacetamide (IAA; Sigma-Aldrich). Proteins were separated by 4−12% Bis-Tris gradient gels (NuPAGE, Invitrogen, ThermoFisher Scientific) and protein lanes were divided into 10 fractions. Proteins from the gel pieces were digested with trypsin HPLC-grade (Promega AG, Dübendorf, Switzerland) overnight and the resulting peptide solutions were desalted on C18-based STAGE tips as previously described [50,51]. Samples were analyzed by an LTQ Orbitrap XL mass spectrometer (ThermoFisher Scientific) coupled to an Agilent 1200 nano flow-HPLC, as well as by a QExactive mass spectrometer (Thermo Fisher Scientific), coupled to an Easy nanoLC (ThermoFisher Scientific). HPLC column tips (fused silica, 75 μm inner diameter, 20 cm final length) were in-house packed with Reprosil-Pur 120 C18-AQ, 3 or 1.9 μm (Dr. Maisch). A gradient of buffer A (0.5% acetic acid; Sigma-Aldrich) and B (0.5% acetic acid in 80% acetonitrile; LGC Standards-Promochem, Wesel, Germany) with increasing organic proportion

was used for peptide separation. For the LTQ Orbi-trap samples were separated within 145 min (linear gradient of buffer B from 10 to 80% within 110 min). On the Easy nanoLC, samples were separated for 50 min (5−25% buffer *B* in 37 min, increase to 50% at 45 min, and complete elution at 80% buffer *B*). The flow rates were set to 250 nl×min^{-1}. The spray voltage was 2.3 kV . The capillary temperature was set to 200 °C for the LTQ Orbitrap XL and 250 °C for the QExactive. No sheath or auxiliary gas flow was used. Data acquisition was done data-dependent: the MS switched automatically between MS (max. 1×10^6 ions) and a maximum of five MS/MS scans (10 MS/MS scans on the QExactive). The collision energy in the linear ion trap was set to 35% (25% for the QExactive) and a target value of 5'000 parent ions. The scan range for the LTQ Orbitrap XL was set to 350−2000 m/z with a resolution of 60'000. For the QExactive the scan range was set to 200−2000 m/z with a resolution of 70'000. Parent ions with an unassigned charge or a charge state of $z = 1$ were excluded from fragmentation.

Protein identification and relative quantification

Peak detection and relative quantification of SILAC-pairs was conducted by MaxQuant version 1.4.1.2 [52]. Peaks were searched against a full-length human Uniprot database from December

2017. Enzyme specificity was assigned to trypsin/P and quantitation was based on three SILAC labels. Carbamidomethylation was set as a fixed modification; N-terminal acetylation and oxidation of methionine, as well as phosphorylations of serine/threonine and tyrosine were set as variable modifications. The MS/MS tolerance was set to 0.5 Da. A maximum of two missed cleavages was allowed. Proteins were identified with a minimum of one unique peptide. For quantification, a ratio count of two was needed. Identification and quantification of peptides and proteins was based on a reverse-database with a false discovery rate (FDR) of 0.01. Peptide length had to be at least 7 amino acids. Identified peptides were re-quantified. For enhanced identification, runs were matched with a match time window of 1 min. For the data analysis, normalized protein ratios were evaluated using Perseus 1.5.5.3 [53]. Contaminants, reverse hits and proteins only identified by site were excluded from further analysis. To eliminate unspecific enriched proteins, Significance A with a Benjamini-Hochberg corrected FDR of 0.05 was calculated for normalized, log2-transformed ratios. Only proteins with a significant enrichment in at least one experiment were used for subsequent analysis. The ratios were z-normalized and k-means clustered in MeV (Multi Experiment viewer) [27]. Enriched GO-terms (FDR = 0.05) in 5 different clusters were identified in STRING version 10.5 [54].

Western blot analysis

Normal and RDEB-derived fibroblasts were cultured in 6-cm plates or 6-well plates until they reached ~70% confluence. Cells were serum-starved overnight (0.25% FBS) prior to stimulation with PDGF-BB or TGFβ. Cells were lysed with modified RIPA buffer (50 mM Tris-HCl pH 7.5, 150 mM NaCl, 1 mM EDTA, 1% NP-40, 0.25% deoxycholic acid; Sigma-Aldrich) supplemented with proteases and phosphatases inhibitors. Lysates were centrifuged at 12000 rpm for 15 min at 4 °C. Protein concentration was determined by pierce BCA protein assay kit and, when possible, samples containing 30 μg protein were prepared in Laemmli loading buffer containing 1mM DTT. Samples were heated 10 min at 75 °C. Proteins were separated in SDS-PAGE gels and transferred to 0.2 μm PVDF membranes (Amersham™ Hybond™ Protran). The membranes were blocked during 1 h in 5% BSA or 5% non-fat milk prepared in TBS with 0.1% Tween-20 (TBST) and they were incubated overnight at 4 °C with the following primary antibodies and dilutions: anti-phospho-Tyrosine (4G10) (1:1000), anti-PDGFRβ (D-6) (1:500), anti-Cbl-b (1:1000), anti-c-Cbl (1:1000), anti-phospho-ERK 1/2 (1:2000), anti-ERK 1/2 (1:1000), anti-phospho-Akt (1:1000), anti-Akt (1:1000), anti-phospho-Smad3 (1:2000), anti-

Smad3 (1:1000) and anti-GAPDH (1:1000) as loading control. The next day, blots were incubated 1 h at room temperature with goat anti-rabbit (1:10000) or anti-mouse (1:5000) HRP-conjugated secondary antibodies (Jackson ImmunoResearch Europe Ltd, Newmarket, UK) and signal was detected with WesternBright ECL Spray (Advansta, Menlo Park, CA, USA) or SuperSignal West Femto Maximum Sensitivity Substrate (ThermoFisher Scientific) in Odyssey® Fc Imaging System (LI-COR Biosciences, Lincoln, NE). Densitometric analysis for quantification were done with Image-J (NIH) software.

PDGFRβ ubiquitination levels

Normal and RDEB-derived fibroblasts were cultured in 10-cm plates until they reached 90% confluence. Cells were serum-starved overnight prior to 3 min stimulation with 15 ng/mL PDGF-BB. Cells were lysed for 30 min at 4 °C on the wheel with RIPA buffer (50 mM Tris-HCl pH 8.0, 150 mM NaCl, 1% NP-40, 0.5% deoxycholic acid, 0.1% SDS, 2 mM MgCl₂; Sigma-Aldrich) supplemented with proteases and phosphatases inhibitors and 50 mM 2-Chloroacetamide to inhibit the de-ubiquitinases. Lysates were centrifuged at 12000 rpm for 15 min at 4 °C. Protein concentration was determined by pierce BCA protein assay kit and 500 μg of protein lysates were used as starting material for immunoprecipitation. Protein extracts were incubated overnight with 1 μg of anti-PDGFRβ (D-6) antibody and immunocomplexes recovered using 25 μL Protein G Sepharose beads (Sigma) for 1 h 30 min in the wheel at 4 °C. The beads were washed with RIPA buffer and proteins were eluted in 2x Laemmli buffer supplemented with 1 mM DTT and boiled 5 min at 95 °C. Western blots were performed as stated before and the membranes were incubated overnight at 4 °C with the following primary antibodies and dilutions: anti-ubiquitin (1:1000) and anti-PDGFRβ (28E1) (1:1000). For analysis of whole cell lysates, 30 μg of protein lysates were used and membranes were incubated with anti-PDGFRβ (D-6) (1:500) and anti-GAPDH (1:1000) as loading control. The next day, blots were incubated 1 h at room temperature with goat anti-rabbit (1:10000), anti-mouse (1:5000) or anti-mouse light chain (1:10000) HRP-conjugated secondary antibodies and signal was detected as described above (see Western Blot analysis). Densitometric analysis was done with Image-J (NIH) software and ubiquitination levels were normalized to the corresponding levels of immunoprecipitated PDGFRβ.

Confocal microscopy

Cells were cultured on collagen I pre-coated coverslips disposed on 24-well plates. 15000 fibroblasts per condition were cultured and they were serum-

starved overnight prior to stimulation with 15 ng/mL PDGF-BB for 0, 5 and 10 min. After treatment, cells were fixed with parafolmaldehyde (PFA) 4% for 15 min and washed with PBS. Blocking and permeabilization was performed with 10% goat serum prepared in PBS with 0.25% Triton X-100 (Sigma-Aldrich). Cells were incubated with anti-PDGFRβ (28E1) (1:100) and anti-SNX1 (1:100) overnight at 4 °C in a humid chamber. Coverslips were washed with PBS with 0.25% triton X-100 and followed by incubation with secondary antibodies Alexa Fluor 488 anti-rabbit and Alexa Fluor 594 anti-mouse (1:1000) together with Hoechst 33342 1 μM (14533; Sigma-Aldrich) for nuclei staining for 1 h at room temperature. Coverslips were mounted on glass slides with ProLong Gold antifade reagent (P36930; ThermoFisher Scientific) and the edges were sealed with nail polish. For Smad3 staining, prior to blocking, fixed cells were incubated 20 min at 55 °C with 10 mM sodium citrate buffer (pH 6) for antigen retrieval, followed by 10 min incubation on ice. Afterwards, normal protocol was followed. Cells were incubated with anti-Smad3 (1:100) overnight at 4 °C in a humid chamber and Alexa Fluor 488 anti-rabbit (1:1000) was used as secondary antibody together with Hoechst 33342 1 μM for nuclei staining during 1 h at room temperature. Cells were visualized by inverted microscopy. Images of the specimens were collected with a TCS SPE-II confocal microscope (Leica Microsystems, Wetzlar, Germany), equipped with 63×/1.3 oil-immersion objective. *Z*-series images were obtained through the collection of serial confocal sections at 0.4 μm intervals. To compare the confocal data, identical confocal settings were used for image acquisition of different experiments. Quantitative co-localization analysis of PDGFRβ and SNX1 was performed with Imaris x64 v7.2.1 software (BITPLANE, Oxford Instruments), using object-based co-localization. For generation of SNX1 and PDGFRβ spots, particle size was measured and determined to 0.4 μm. The minimum distance between spots was set to 0.4 μm (distance from the center of spots), meaning that the spots have to be in touch for considering them as co-localizing particles. Finally, the number of co-localized spots were counted per cell.

Nuclear localization of Smad3 was quantified using Image-J (NIH) software. Briefly, plot profiles of Smad3 intensity per cell along cell diagonals were generated by measuring the fluorescence intensity using the Plot Profile tool and respective z-stacks. Local maxima of fluorescence intensities reflecting nuclear staining were summed and quantified compared to total signal intensities for each profile.

BrdU-based cell viability assay

Cells were cultured in 96-well plates and they were serum deprived overnight. Cells were treated with 25 ng/mL of PDGF-BB together with BrdU in low-serum DMEM. After 24 h incubation, the reaction was stopped and the incorporation of BrdU was detected with an HRP-secondary antibody, according to the manufacturer's recommendations (BrdU Cell Proliferation ELISA Kit, Abcam).

Cell migration assay

Normal and RDEB-derived fibroblasts were cultured in 96-well plates and they were grown until they reached full confluence. Cells were serum-starved overnight and the following day they were pre-incubated with 1 μg/mL mitomycin C (CAS 50-07-7, sc-3514A; Santa Cruz Biotechnologies) 1 h prior to the scratch generation to block proliferation. The scratch was performed with the IncuCyte® 96-well WoundMaker Tool (Essen Biosciences; Newark, UK). Cells were washed twice with low-serum DMEM and finally they were stimulated with vehicle or 5 ng/mL PDGF-BB in presence of 1 μg/mL mitomycin C. The motility of cells was monitored during 30 h by time-lapse video microscopy using the Incucyte® Live Cell analysis system (Essen Biosciences). Quantification of wound closure was performed using the plugin "MRI-wound healing" developed for Image-J (NIH) software. In each experiment, wound closure data was normalized to the respective control, corresponding to the width at 0 h.

mRNA Isolation and Reverse Transcriptase qRT-PCR

NHF and RDEB fibroblasts were treated with 10 ng/mL TGF-β and/or 5 μM of the TGF-β receptor type I/II (TβRI/II) dual inhibitor LY210976 for the indicated timepoints. RNA was isolated with RNeasy Mini kit (Qiagen, Hilden, Germany) following manufacturer's guidelines. Reverse transcription was performed with Quantitect RT kit (Qiagen), using 400 ng RNA as starting material. Quantitative PCR was then performed using the KAPA SYBR Fast (Universal) qPCR kit (Merck Millipore) according to the manufacturer's recommendations. The qRT-PCR reaction was performed with a Rotor-GeneQ (Qiagen) and the same thermal profile conditions were used for all primer sets: 95°C for 10 min; then 40 cycles were performed of 10 s at 95 °C, 20 s 60 °C and 20 s 72 °C. The following primer pairs were used: *CBLB* forward 5′-GCA AGT GGC CAA GTT CCT TT-3′, *CBLB* reverse 5′-TGC CTG TGA ACC ATC TGA; *HPRT1* forward 5′-TGA CAC TGG CAA AAC AAT GCA-3′, *HPRT1* reverse 5′-GGT CCT TTT CAC CAG CAA GCT-3′.

Statistical analysis

Graph-Pad Prism 6 software (GraphPad, La Jolla, CA) was used for graphs generation and statistical

analysis. Data are presented as mean ± s.e. (standard error) of the number of indicated experiments, unless otherwise mentioned. Appropriate statistical tests were performed based on the compared experimental conditions, including Student *t*-test (computed with FDR ≤ 0.05 for correcting for multiple testing when necessary), one-way or two-way analysis of variance (ANOVA). Throughout the paper, statistically significant differences are indicated by: *$p \leq 0.05$, ** $p \leq 0.01$ and *** $p \leq 0.001$.

Data availability statement

The mass spectrometry proteomic data are publicly available and have been deposited to the ProteomeXchange Consortium via the PRIDE partner repository [55] with the dataset identifier PXD022985.

Declaration of Competing Interest

The authors state no conflict of interest.

Funding

Supplementary materials

Supplementary material associated with this article can be found in the online version at doi:10.1016/j.matbio.2021.10.004.

References

[1] J.D. Fine, L. Bruckner-Tuderman, R.A.J. Eady, E.A. Bauer, J.W. Bauer, C. Has, A. Heagerty, H. Hintner, A. Hovnanian, M.F. Jonkman, I. Leigh, M.P. Marinkovich, A.E. Martinez, J.A. McGrath, J.E. Mellerio, C. Moss, D.F. Murrell, H. Shimizu, J. Uitto, D. Woodley, G. Zambruno, Inherited epidermolysis bullosa: updated recommendations on diagnosis and classification, J. Am. Acad. Dermatol. 70 (2014) 1103–1126.

[2] A. Nyström, L. Bruckner-Tuderman, Injury- and inflammation-driven skin fibrosis: the paradigm of epidermolysis bullosa, Matrix Biol. 68−69 (2018) 547–560.

[3] E.S. Gorell, N. Nguyen, Z. Siprashvili, M.P. Marinkovich, A.T. Lane, Characterization of patients with dystrophic epidermolysis bullosa for collagen VII therapy, Br. J. Dermatol. 173 (2015) 821–823.

[4] A.W. Li, B. Prindaville, S.T. Bateman, T.E. Gibson, K. Wiss, Inpatient management of children with recessive dystrophic epidermolysis bullosa: a review, Pediatr. Dermatol. 34 (2017) 647–655.

[5] P. Benny, C. Badowski, E.B. Lane, M. Raghunath, Making more matrix: enhancing the deposition of dermal-epidermal junction components in vitro and accelerating organotypic skin culture development, using macromolecular crowding, Tissue Eng. Part A 21 (2015) 183–192.

[6] F. Cianfarani, G. Zambruno, D. Castiglia, T. Odorisio, Pathomechanisms of altered wound healing in recessive dystrophic epidermolysis bullosa, Am. J. Pathol. 187 (2017) 1445–1453.

[7] R. Bernasconi, K. Thriene, E. Romero-Fernández, C. Gretzmeier, T. Kühl, M. Maler, P. Nauroy, S. Kleiser, A. Rühl-Muth, M. Stumpe, D. Kiritsi, S.F. Martin, B. Hinz, L. Bruckner-Tuderman, J. Dengjel, A. Nyström, Pro-inflammatory immunity supports fibrosis advancement in epidermolysis bullosa: intervention with Ang-(1-7), EMBO Mol. Med. (2021).

[8] V.R. Mittapalli, J. Madl, S. Löffek, D. Kiritsi, J.S. Kern, W. Römer, A. Nyström, L. Bruckner-Tuderman, Injury-driven stiffening of the dermis expedites skin carcinoma progression, Cancer Res. 76 (2016) 940–951.

[9] L. Boltzmann, C. Gruber, A. Klausegger, A. Trost, B. Bogner, H. Reitsamer, J.W. Bauer, Pseudosyndactyly-an inflammatory and fibrotic wound healing disorder in recessive dystrophic epidermolysis bullosa, JDDG J. Ger. Soc. Dermatol. 13 (2015) 1257–1266.

[10] L. Guerra, T. Odorisio, G. Zambruno, D. Castiglia, Stromal microenvironment in type VII collagen-deficient skin: the ground for squamous cell carcinoma development, Matrix Biol. 63 (2017) 1−10.

[11] L. Bruckner-Tuderman, Skin fragility: perspectives on evidence-based therapies, Acta Derm. Venereol. 100 (2020).

[12] A. Nyström, R. Bernasconi, O. Bornert, Therapies for genetic extracellular matrix diseases of the skin, Matrix Biol. 71−72 (2018) 330–347.

[13] E. Rashidghamat, J.A. McGrath, Novel and emerging thera-
     pies in the treatment of recessive dystrophic epidermolysis
     bullosa, Intractable Rare Dis. Res. 6 (2017) 6–20.
[14] D.T. Woodley, M. Chen, Recessive dystrophic epidermolysis
     bullosa: advances in the laboratory leading to new therapies,
     J. Invest. Dermatol. 135 (2015) 1705–1707.
[15] P. Martin, Wound healing - aiming for perfect skin regenera-
     tion, Science 276 (1997) 75–81 (80-.).
[16] C.H. Heldin, J. Lennartsson, B. Westermark, Involvement of
     platelet-derived growth factor ligands and receptors in tumor-
     igenesis, J. Intern. Med. 283 (2018) 16–44.
[17] L. Fredriksson, H. Li, U. Eriksson, The PDGF family: four
     gene products form five dimeric isoforms, Cytokine Growth
     Factor Rev. 15 (2004) 197–204.
[18] Y. Wang, S.D. Pennock, X. Chen, A. Kazlauskas, Z. Wang,
     Platelet-derived growth factor receptor-mediated signal
     transduction from endosomes, J. Biol. Chem. 279 (2004)
     8038–8046.
[19] S. Miyake, K.P. Mullane-Robinson, N.L. Lill, P. Douillard,
     H. Band, Cbl-mediated negative regulation of platelet-
     derived growth factor receptor-dependent cell proliferation. a
     critical role for Cbl tyrosine kinase-binding domain, J. Biol.
     Chem. 274 (1999) 16619–16628.
[20] C. Rorsman, M. Tsioumpekou, C.H. Heldin, J. Lennartsson,
     The ubiquitin ligases c-Cbl and Cbl-b negatively regulate
     platelet-derived growth factor (PDGF) BB-induced chemo-
     taxis by affecting PDGF receptor β (PDGFRβ) internalization
     and signaling, J. Biol. Chem. 291 (2016) 11608–11618.
[21] C. Hellberg, C. Schmees, S. Karlsson, A. Åhgren,
     C.H. Heldin, Activation of protein kinase C α is necessary for
     sorting the PDGF β-receptor to Rab4a-dependent recycling,
     Mol. Biol. Cell. 20 (2009) 2856–2863.
[22] J.C. Bonner, Regulation of PDGF and its receptors in
     fibrotic diseases, Cytokine Growth Factor Rev. 15 (2004)
     255–273.
[23] J. Gotzmann, A.N.M. Fischer, M. Zojer, M. Mikula, V. Proell,
     H. Huber, M. Jechlinger, T. Waerner, A. Weith, H. Beug,
     W. Mikulits, A crucial function of PDGF in TGF-β-mediated
     cancer progression of hepatocytes, Oncogene 25 (2006)
     3170–3185.
[24] A.N.M. Fischer, E. Fuchs, M. Mikula, H. Huber, H. Beug,
     W. Mikulits, PDGF essentially links TGF-beta signaling to
     nuclear beta-catenin accumulation in hepatocellular carci-
     noma progression, Oncogene 26 (2007) 3395–3405.
[25] M. AlQudah, T.M. Hale, M.P. Czubryt, Targeting the renin-
     angiotensin-aldosterone system in fibrosis, Matrix Biol.
     91−92 (2020) 92–108.
[26] G.F. Pierce, J.E. Tarpley, J. Tseng, J. Bready, D. Chang,
     W.C. Kenney, R. Rudolph, M.C. Robson, J. Vande Berg,
     P. Reid, S. Kaufman, C.L. Farrell, Detection of platelet-
     derived growth factor (PDGF)-AA in actively healing human
     wounds treated with recombinant PDGF-BB and absence of
     PDGF in chronic nonhealing wounds, J. Clin. Invest. 96
     (1995) 1336–1350.
[27] A.I. Saeed, V. Sharov, J. White, J. Li, W. Liang,
     N. Bhagabati, J. Braisted, M. Klapa, T. Currier,
     M. Thiagarajan, A. Sturn, M. Snuffin, A. Rezantsev,
     D. Popov, A. Ryltsov, E. Kostukovich, I. Borisovsky, Z. Liu,
     A. Vinsavich, V. Trush, J. Quackenbush, TM4: A free, open-
     source system for microarray data management and analy-
     sis, Biotechniques 34 (2003) 374–378.
[28] R.C. Kurten, D.L. Cadena, G.N. Gill, Enhanced degradation
     of EGF receptors by a sorting nexin SNX1, Science 272
     (1996) 1008–1010 (80-.).
[29] C.A. Worby, J.E. Dixon, Sorting out the cellular functions of
     sorting nexins, Nat. Rev. Mol. Cell Biol. 3 (2002) 919–931.
[30] J.B. Demoulin, A. Essaghir, PDGF receptor signaling net-
     works in normal and cancer cells, Cytokine Growth Factor
     Rev. 25 (2014) 273–283.
[31] J.A. McCubrey, L.S. Steelman, W.H. Chappell, S.L. Abrams,
     E.W.T. Wong, F. Chang, B. Lehmann, D.M. Terrian,
     M. Milella, A. Tafuri, F. Stivala, M. Libra, J. Basecke,
     C. Evangelisti, A.M. Martelli, R.A. Franklin, Roles of the Raf/
     MEK/ERK pathway in cell growth, malignant transformation
     and drug resistance, Biochim. Biophys. Acta Mol. Cell Res.
     1773 (2007) 1263–1284.
[32] T.F. Franke, S. Il Yang, T.O. Chan, K. Datta, A. Kazlauskas,
     D.K. Morrison, D.R. Kaplan, P.N. Tsichlis, The protein kinase
     encoded by the Akt proto-oncogene is a target of the PDGF-acti-
     vated phosphatidylinositol 3-kinase, Cell 81 (1995) 727–736.
[33] B.D. Manning, A. Toker, AKT/PKB Signaling, Navigating the
     network, Cell 169 (2017) 381–405.
[34] A. Nyström, D. Velati, V.R. Mittapalli, A. Fritsch, J.S. Kern,
     L. Bruckner-Tuderman, Collagen VII plays a dual role in
     wound healing, J. Clin. Invest. 123 (2013) 3498–3509.
[35] T. Odorisio, M. Di Salvio, A. Orecchia, G. Di Zenzo,
     E. Piccinni, F. Cianfarani, A. Travaglione, P. Uva, B. Bellei,
     A. Conti, G. Zambruno, D. Castiglia, Monozygotic twins dis-
     cordant for recessive dystrophic epidermolysis bullosa phe-
     notype highlight the role of TGF-β signalling in modifying
     disease severity, Hum. Mol. Genet. 23 (2014) 3907–3922.
[36] A. Nyström, K. Thriene, V. Mittapalli, J.S. Kern, D. Kiritsi,
     J. Dengjel, L. Bruckner-Tuderman, Losartan ameliorates
     dystrophic epidermolysis bullosa and uncovers new disease
     mechanisms, EMBO Mol. Med. 7 (2015) 1211–1228.
[37] V. Küttner, C. MacK, K.T.G. Rigbolt, J.S. Kern, O. Schilling,
     H. Busch, L. Bruckner-Tuderman, J. Dengjel, Global remod-
     elling of cellular microenvironment due to loss of collagen
     VII, Mol. Syst. Biol. (2013) 9.
[38] M.R. Crowley, D. Bowtell, R. Serra, TGF-β, c-Cbl, and
     PDGFR-α the in mammary stroma, Dev. Biol. 279 (2005)
     58–72.
[39] D. R, Z. Y, F. XH, Smads: transcriptional activators of TGF-
     beta responses, Cell 95 (1998) 737–740.
[40] A. Östman, PDGF receptors-mediators of autocrine tumor
     growth and regulators of tumor vasculature and stroma,
     Cytokine Growth Factor Rev. 15 (2004) 275–286.
[41] M. Demaria, N. Ohtani, S.A. Youssef, F. Rodier,
     W. Toussaint, J.R. Mitchell, R.M. Laberge, J. Vijg,
     H. VanSteeg, M.E.T. Dollé, J.H.J. Hoeijmakers, A. deBruin,
     E. Hara, J. Campisi, An essential role for senescent cells in
     optimal wound healing through secretion of PDGF-AA, Dev.
     Cell. 31 (2014) 722–733.
[42] K.Y. DeLeon-Pennell, T.H. Barker, M.L. Lindsey, Fibroblasts:
     the arbiters of extracellular matrix remodeling, Matrix Biol.
     91−92 (2020) 1–7.
[43] V. Akimov, M. Fehling-Kaschek, I. Barrio-Hernandez,
     M. Puglia, J. Bunkenborg, M.M. Nielsen, J. Timmer,
     J. Dengjel, B. Blagoev, Magnitude of ubiquitination deter-
     mines the fate of epidermal growth factor receptor upon
     ligand stimulation, J. Mol. Biol. 433 (2021) 167240.
[44] J.D. Weber, D.M. Raben, P.J. Phillips, J.J. Baldassare, Sus-
     tained activation of extracellular-signal-regulated kinase 1
     (ERK1) is required for the continued expression of cyclin D1
     in G1 phase, Biochem. J. 326 (1997) 61–68.
[45] L.O. Murphy, S. Smith, R.H. Chen, D.C. Fingar, J. Blenis,
     Molecular, interpretation of ERK signal duration by immedi-
     ate early gene products, Nat. Cell Biol. 4 (2002) 556–564.

[46] Y.Z. Ng, C. Pourreyron, J.C. Salas-Alanis, J.H.S. Dayal, R. Cepeda-Valdes, W. Yan, S. Wright, M. Chen, J.D. Fine, F.J. Hogg, J.A. McGrath, D.F. Murrell, I.M. Leigh, E.B. Lane, A.P. South, Fibroblast-derived dermal matrix drives development of aggressive cutaneous squamous cell carcinoma in patients with recessive dystrophic epidermolysis bullosa, Cancer Res. 72 (2012) 3522–3534.

[47] J. Kosla, M. Dvorakova, M. Dvorak, V. Cermak, Effective myofibroblast dedifferentiation by concomitant inhibition of TGF-β signaling and perturbation of MAPK signaling, Eur. J. Cell Biol. 92 (2013) 363–373.

[48] J. Doukas, L.A. Chandler, A.M. Gonzalez, D. Gu, D.K. Hoganson, C. Ma, T. Nguyen, M.A. Printz, M. Nesbit, M. Herlyn, T.M. Crombleholme, S.L. Aukerman, B.A. Sosnowski, G.F. Pierce, Matrix immobilization enhances the tissue repair activity of growth factor gene therapy vectors, Hum. Gene Ther. 12 (2001) 783–798.

[49] J.S. Kern, J. Kohlhase, L. Bruckner-Tuderman, C. Has, Expanding the COL7A1 mutation database: novel and recurrent mutations and unusual genotype - Phenotype constellations in 41 patients with dystrophic epidermolysis bullosa, J. Invest. Dermatol. 126 (2006) 1006–1012.

[50] A. Shevchenko, H. Tomas, J. Havliš, J.V. Olsen, M. Mann, In-gel digestion for mass spectrometric characterization of proteins and proteomes, Nat. Protoc. 1 (2007) 2856–2860.

[51] J. Rappsilber, M. Mann, Y. Ishihama, Protocol for micro-purification, enrichment, pre-fractionation and storage of peptides for proteomics using stagetips, Nat. Protoc. 2 (2007) 1896–1906.

[52] J. Cox, M. Mann, MaxQuant enables high peptide identification rates, individualized p.p.b.-range mass accuracies and proteome-wide protein quantification, Nat. Biotechnol. 26 (2008) 1367–1372.

[53] S. Tyanova, T. Temu, P. Sinitcyn, A. Carlson, M.Y. Hein, T. Geiger, M. Mann, J. Cox, The Perseus computational platform for comprehensive analysis of (prote)omics data, Nat. Methods 13 (2016) 731–740.

[54] D. Szklarczyk, A. Franceschini, S. Wyder, K. Forslund, D. Heller, J. Huerta-Cepas, M. Simonovic, A. Roth, A. Santos, K.P. Tsafou, M. Kuhn, P. Bork, L.J. Jensen, C. von Mering, STRING v10: protein-protein interaction networks, integrated over the tree of life, Nucleic Acids Res. 43 (2015) D447–D452.

[55] J.A. Vizcaíno, A. Csordas, N. Del-Toro, J.A. Dianes, J. Griss, I. Lavidas, G. Maye, Y. Perez-Riverol, F. Reisinger, T. Ternent, Q.W. Xu, R. Wang, H. Hermjakob, 2016 Update of the PRIDE database and its related tools, Nucleic Acids Res. 44 (2016) D447–D456.